2011 American Control Conference
on O'Farrell Street, San Francisco, CA, USA
June 29 - July 01, 2011

Approximate Solutions to Nonlinearly-Constrained Optimal Control Problems

Philip S. Harvey and Henri P. Gavin

Abstract— **The use of variational methods in optimal control problems involves solving a two-point boundary-value problem (for states and costates) and satisfying an optimality condition. For problems with quadratic integral cost that have linear state dynamics and unconstrained controls, the co-state equations are also linear. Adjoining control constraints to the objective function introduces non linearity to the costate equation, and iterative numerical methods are required to converge upon the optimal control trajectory. The nonlinear costate terms arise at times in which the control constraints are active. In the numerical methodology proposed in this paper, an approximately optimal solution is converged upon from a feasible suboptimal initial control trajectory. In each iteration the control trajectory moves toward the unconstrained optimum solution while remaining feasible. Importantly, the state and costate equations are linear and the method is applied to a multi-input system designed to minimize the response of a vibration isolation system by adjusting only the damping characteristics of a variable damping device.**

I. INTRODUCTION

In the time domain, the solution to nonlinear optimal control problems involves solving a two-point boundary value problem posed by the Euler-Lagrange equations [1]. For most nonlinear problems, solutions are iteratively converged upon. Problems involving inequality constraints on the controls and states are representative of a wide range of applications but remain open problems. For a quadratic performance index and constraints on states and controls, the solution consists of trajectories that are sometimes constrained and are sometimes within their feasible space [2]. Various methods have been proposed to find the optimal solution for linearly constrained problems [3],[4],[5],[6]. One such method uses integral penalty functions to approximately enforce the constraint [7]. This method requires a choice of weighting constant and penalty function. If the weighting constant is too small the actual constraint may not be enforced. This paper presents a numerical method exhibiting monotonic convergence to the optimal control trajectories for a linear system with nonlinear sector bound constraints on the controls and states.

Semi-active control is a class of control systems in which a small amount of external power is required to modulate mechanical properties of the actuators (i.e., stiffness and damping) [8],[9],[10],[11]. The circle criterion guarantees the absolute stability of semi-active control systems; the plant dynamics are typically linear with strictly positive-real transfer functions and the control forces are sector-bounded (within quadrants I and III in the velocity-force plane) [12]. Implementation of semi-active control involves controls acting through actuators that exhibit saturation limits. Therefore, the controls are sector-bounded.

In this study, trajectories for optimal damping rates are calculated for equipment isolation systems that operate on the principle of a rolling pendulum. The isolated components are supported by large ball bearings (2 cm in diameter) that roll on rigid dish-shaped bowls with a quadratic profile. The period of motion is determined by the curvature of the dish, independent of the mass. Damping force is modulated in the isolation system in order to minimize a quadratic performance functional that weights total response accelerations and control efforts in order to improve the isolation system transmissibility at high frequencies while simultaneously suppressing resonant behavior. This method requires a priori knowledge of the disturbance and cannot be implemented in non-autonomous systems. However, from the optimal control trajectories, parameterized feedback control laws may be deduced.

The economic impact of earthquakes depends not only on the performance of primary structural components, but also the performance of non-structural building contents. The serviceability of many important facilities (e.g., hospitals, emergency-response centers, computer centers etc.) depend on the functionality of non-structural components following an earthquake even when the facility's structural system remains operational [13],[14],[15],[16]. Therefore, seismic hazards analyses of structures must include the effects damage to critical equipment [16],[17]. Failure of vibration-sensitive equipment is caused not only by overturning or toppling, but also by excessive displacements and/or large absolute equipment accelerations. For this reason vibration isolation systems are installed to mitigate the seismic risk posed to mission-critical equipment.

Isolation systems can considerably reduce the base acceleration transmitted to objects by mechanically decoupling the isolator from the ground [8],[17]. Seismic equipment isolation systems are typically of two types—friction-pendulum or rolling-pendulum [18],[19],[20]—with natural periods between 2 and 4 s [13],[17]. During low-level seismic events, passive equipment isolation systems perform extremely well [9],[21],[22],[23]. Whereas, when subjected to earthquakes with high-amplitude near-fault ground motions, considerable amplification will produce excessive isolator displacements

This work was not supported by any organization

P.S. Harvey is with Department of Civil and Environmental Engineering, Duke Univ., Durham, NC 27708-0287, USA Philip.Harvey@duke.edu

H.P. Gavin is with the Faculty of Department of Civil and Environmental Engineering, Duke Univ., Durham, NC 27708-0287, USA Henri.Gavin@duke.edu

endangering the isolated object [9]. Passive damping is effective in reducing isolator drifts but at the expense of increasing equipment accelerations at high frequencies [24]. Another drawback of passive damping is the inability to adjust system parameters to achieve the desired performance objectives without a priori knowledge of the external excitation. Therefore, it would be desirable to be able to adaptively adjust system parameters in order to optimize the performance of equipment isolation systems for both near- and far- field ground motions. To this end, structural control, or smart isolation systems, has been proposed. In particular semi-active control systems are attractive due to their guaranteed stability and low power consumption [13],[17],[25].

II. METHOD

A. Euler-Lagrange Equations

An admissible control trajectory $\mathbf{u}(t)$, $t_0 \le t \le t_f$, is to be applied to a non-autonomous system

$$\dot{\mathbf{x}}(t) = \mathbf{f}[\mathbf{x}, \mathbf{u}; t], \;\; \mathbf{x}(t_0) = \mathbf{x}_0, \;\; \mathbf{x} \in \mathbb{R}^n, \;\; \mathbf{u} \in \mathbb{R}^m \qquad (1)$$

in order to minimize a Lagrange-type cost function of the states and control

$$J = \int_{t_0}^{t_f} \mathcal{L}[\mathbf{x}, \mathbf{u}; t]\, dt \;, \qquad (2)$$

subject to the constraints of the system dynamics (1) and the l-component state-control inequality constraint

$$\mathbf{c}[\mathbf{u}, \mathbf{x}; t] \le \mathbf{0} \;. \qquad (3)$$

This is accomplished by minimizing the first variation of an augmented cost,

$$J_A = \int_{t_0}^{t_f} \left\{ \mathcal{L} + \mathbf{p}^T(t) \left(\mathbf{f} - \dot{\mathbf{x}} \right) + \lambda^T(t) \mathbf{c} \right\} \, dt \qquad (4)$$

where $\mathbf{p}(t)$ are the costates and $\lambda(t)$ are Lagrange multipliers for the inequality constraint (3). Defining the Hamiltonian,

$$\mathcal{H} = \mathcal{L} + \mathbf{p}^T \mathbf{f} + \lambda^T \mathbf{c} \;\; \text{where} \;\; \begin{array}{l} \lambda = \mathbf{0} \text{ if } \mathbf{c} < \mathbf{0} \\ \lambda \ge \mathbf{0} \text{ if } \mathbf{c} = \mathbf{0} \end{array} \qquad (5)$$

the necesary condition for control optimality is found from the first variation of J_A

$$\frac{\partial \mathcal{H}}{\partial \mathbf{u}} : \; \mathbf{0} = \left(\frac{\partial \mathcal{L}}{\partial \mathbf{u}} \right)^T + \left[\frac{\partial \mathbf{f}}{\partial \mathbf{u}} \right]^T \mathbf{p} + \left[\frac{\partial \mathbf{c}}{\partial \mathbf{u}} \right]^T \lambda \qquad (6)$$

in which the co-state equation is

$$\frac{\partial \mathcal{H}}{\partial \mathbf{x}} : \; \dot{\mathbf{p}} = - \left(\frac{\partial \mathcal{L}}{\partial \mathbf{x}} \right)^T - \left[\frac{\partial \mathbf{f}}{\partial \mathbf{x}} \right]^T \mathbf{p} - \left[\frac{\partial \mathbf{c}}{\partial \mathbf{x}} \right]^T \lambda \qquad (7)$$

where $\mathbf{p}(t_f) = \mathbf{0}$. Equations (6) and (7) are the Euler-Lagrange equations for a system with constraints on states and controls.

B. Enforcing constraints with Lagrange multipliers

A numerical solution to the Euler-Lagrange equations is found by solving the two-point boundary value problem by iterative modification. At iteration (k), four trajectories—$\mathbf{u}^k(t)$, $\mathbf{x}^k(t)$, $\lambda^k(t)$, and $\mathbf{p}^k(t)$—must be updated from the previous iteration. However, a consistent set updating scheme cannot be determined from (6) and (7). If an inconsistency occurs in the update of the set, the set does not satisfy $\frac{\partial \mathcal{H}}{\partial \mathbf{x}} = 0$, and would not lead to a stationary solution.

This issue motivates the development of an iterative method for solving optimal control problems with nonlinear constraints on the controls and states, in which the controls are initialized to be feasible and remain feasible throughout all iterations. So doing, the Lagrange multipliers are always zero and the costate dynamics at iteration $(k+1)$ involve only the states $\mathbf{x}^{(k+1)}$ allowing for consistent update schemes.

C. Proposed numerical methods for solving Euler-Lagrange equations

Two methods are proposed to enforce the constraint:

1) Method A: Exact adherence to constraints: Consider a linear dynamic system with constant coefficients

$$\dot{\mathbf{x}}(t) = \mathbf{A}\mathbf{x} + \mathbf{B}\mathbf{u} + \mathbf{C}\mathbf{w}, \;\; \mathbf{x}(t_0) = \mathbf{x}_0 \qquad (8)$$

where $\mathbf{w}$ is an uncontrolled input. A quadratic Lagrangian may be expressed as

$$\mathcal{L}[\mathbf{x}, \mathbf{u}; t] = \mathbf{x}^T \mathbf{Q} \mathbf{x} + \mathbf{2 x^T S u} + \mathbf{u^T R u} \qquad (9)$$

where $\mathbf{Q}$ and $\mathbf{R}$ are symmetric. If $\mathbf{c}[\mathbf{u}, \mathbf{x}; t] < \mathbf{0}$ for all time the Lagrange multipliers $\lambda(t)$ are zero and the Euler-Lagrange equations reduce to

$$\mathbf{0} = 2\mathbf{R}\mathbf{u} + 2\mathbf{S}^T \mathbf{x} + \mathbf{B}^T \mathbf{p} \qquad (10)$$

$$\dot{\mathbf{p}} = -2\mathbf{Q}\mathbf{x} - 2\mathbf{S}\mathbf{u} - \mathbf{A}^T \mathbf{p} \;. \qquad (11)$$

Note that both the state and costate dynamics are first order linear ordinary differential equations that may be easily solved by analytical or semi-analytical methods.

An iterative procedure to update the controls, states, and costates is proposed here to converge on the optimal control trajectory. Provided a feasible initial guess for the control trajectory $\mathbf{u}^{(0)}$, equations (8) and (11) can be integrated to find associated state trajectories $\mathbf{x}^{(0)}$ and costate trajectories $\mathbf{p}^{(0)}$, respectively. At iteration (k), a trial control trajectory consistent with $\mathbf{x}^{(k)}$ and $\mathbf{p}^{(k)}$ is found from (10)

$$\tilde{\mathbf{u}}^{(k)}(t) = -\frac{1}{2} \mathbf{R}^{-1} \left(2\mathbf{S}^T \mathbf{x}^{(k)} + \mathbf{B}^T \mathbf{p}^{(k)} \right) \qquad (12)$$

i.e., by setting the gradient of the Hamiltonian equal to zero. Note $\tilde{\mathbf{u}}^{(k)}$ might not be feasible for all time. Consistent states $\mathbf{x}^{(k+1)}$ and controls $\mathbf{u}^{(k+1)}$ are updated simultaneously by solving the state dynamics (8) augmented with saturated controls

$$\mathbf{u}^{(k+1)}(t) = \text{Sat} \left[(1-\gamma)\mathbf{u}^{(k)} + \gamma \text{Sat}[\tilde{\mathbf{u}}^{(k)}, \mathbf{x}^{(k+1)}], \mathbf{x}^{(k+1)} \right] \qquad (13)$$

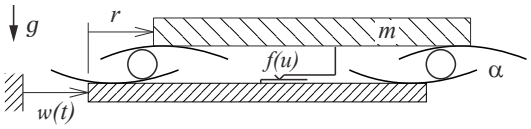

Fig. 1. Schematic of equipment isolation system.

where γ is a positive scalar update gain and $\mathrm{Sat}[\cdot]$ is the saturation operation

$$\mathrm{Sat}\left[\mathbf{u}^{(k)}, \mathbf{x}^{(k)}; t\right] = \begin{cases} \mathbf{u}^{(k)}, & c_j\left[\mathbf{u}^{(k)}, \mathbf{x}^{(k)}; t\right] \leq 0 \\ \hat{\mathbf{u}}^{(k)}, & c_j\left[\mathbf{u}^{(k)}, \mathbf{x}^{(k)}; t\right] > 0 \end{cases}$$
$$\text{s.t. } c_j\left[\hat{\mathbf{u}}^{(k)}, \mathbf{x}^{(k)}; t\right] = 0 \ \forall j \ . \tag{14}$$

(We assume here that no more than one constraint is invoked at any point in time.) Note that the saturation operation makes the state dynamics nonlinear. The costates $\mathbf{p}^{(k+1)}$ are then updated from (11) using $\mathbf{u}^{(k+1)}$ and $\mathbf{x}^{(k+1)}$. The integral cost is accumulated within each iteration and iterations are terminated when criteria are satisfied.

2) Method B: Approximate adherence to constraints: An alternate approach involves linear state dynamics but does not rigorously enforce the inequality constraint on the controls. The states, controls, and costates are initialized in the same manner as before. At iteration (k), the trial control trajectory $\tilde{\mathbf{u}}^{(k)}$ found from (12) is saturated to the feasibility boundary and the controls are updated by an incremental move toward the saturated value.

$$\mathbf{u}^{(k+1)}(t) = (1-\gamma)\mathbf{u}^{(k)}(t) + \gamma \mathrm{Sat}[\tilde{\mathbf{u}}^{(k)}(t), \mathbf{x}^{(k)}(t)] \tag{15}$$

Consistent states $\mathbf{x}^{(k+1)}$ are found by integrating the linear state dynamics, (8), using $\mathbf{u}^{(k+1)}$, and the costates $\mathbf{p}^{(k+1)}$ are then updated from $\mathbf{u}^{(k+1)}$ and $\mathbf{x}^{(k+1)}$.

By saturating the controls with respect to the states $\mathbf{x}^{(k)}$ from the previous iteration, the updated controls are feasible with respect to $\mathbf{x}^{(k)}$ but not necessarily with $\mathbf{x}^{(k+1)}$. Hence, the algorithm does not enforce the constraint strictly, but will keep the controls close the the boundary due to the incremental update of the controls, provided γ is small enough. Because the state dynamics are linear and may be solved using a matrix exponential with faster and more accurate computation, this approximate method is attractive.

III. APPLICATION TO EQUIPMENT ISOLATION SYSTEMS

In this study, optimal control trajectories are found for the single-degree-of-freedom equipment isolation system shown in Figure 1. The linear time-invariant control system is expressed in state space form (8) where the state vector

$$\mathbf{x}(t) = [r(t) \quad \dot{r}(t) \quad f(t)]^T \ . \tag{16}$$

The system matrices $\mathbf{A}$, $\mathbf{B}$, and $\mathbf{C}$ are

$$\mathbf{A} = \begin{bmatrix} 0 & 1 & 0 \\ -g\alpha & 0 & -\frac{1}{m} \\ 0 & 0 & -\frac{1}{T} \end{bmatrix}, \ \mathbf{B} = \begin{bmatrix} 0 \\ 0 \\ \frac{1}{T} \end{bmatrix}, \ \mathbf{C} = \begin{bmatrix} 0 \\ -1 \\ 0 \end{bmatrix}$$

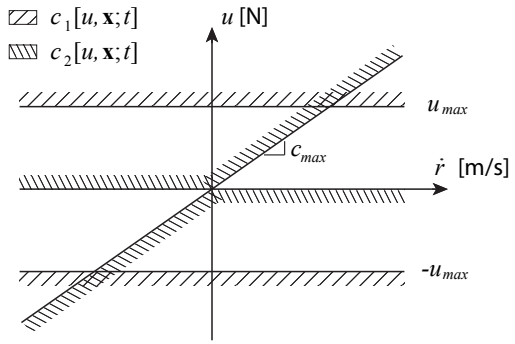

Fig. 2. Sector bound constraint for semi-active damping control.

for parabolic bowl of curvature α, gravitational acceleration g of 9.81 m/s^2, and equipment mass m taken to be 500 kg. The system has a natural period $T_n = 2\pi/\sqrt{g\alpha}$ approximately equal to 2 seconds, for α equal to 1 m^{-1}. The system is forced with base acceleration $w(t)$. The state vector includes the position and velocity of the isolated mass, $r(t)$ and $\dot{r}(t)$.

The third state equation models the dynamics of the controllable damping force $f(t)$ as a function of the control $u(t)$. In this application the damping force is modeled as a controllable internal force and may be interpreted as a friction coefficient acting with time lag $T = 0.02$ s. Feasible control actions are bounded by sectors shown in Figure 2. Constraining the control consequently constrains the damping force. The controllable damper has the performance limitations described by a maximum achievable damping coefficient c_{max} and control force amplitude u_{max}. The nonlinear constraints are

$$\mathbf{c}[u, \mathbf{x}; t] = \begin{bmatrix} (u - u_{max})(u + u_{max}) \\ u\left(\frac{u}{c_{max}} - \dot{r}\right) \end{bmatrix} . \tag{17}$$

In this application we choose to minimize peak total accelerations without using too much control. Thus the quadratic Lagrangian $\mathcal{L}[\cdot]$ is given by

$$\mathcal{L}[\mathbf{x}, u; t] = q(\ddot{r} + w)^2 + u^2 \tag{18}$$

where q is taken to be 1e6.

A. Numerical example

To initialize the controls, a nonlinear feedback control law was used. The feedback control law is

$$u^{(0)}(t) = \begin{cases} \mu c_{max}\dot{r}(t), & |\dot{r}(t)| \leq \frac{u_{max}}{c_{max}} \\ \mu u_{max}\mathrm{sgn}[\dot{r}(t)], & |\dot{r}(t)| > \frac{u_{max}}{c_{max}} \end{cases} \tag{19}$$

where μ is the fraction of the maximum achievable controls, ensuring feasibility on initialization. Initialization requires solving the nonlinear state dynamics with a fourth order Runge-Kutta solver, but subsequent integrations are linear for given control trajectories and a matrix exponential is used to solve the dynamics equations.

For the sector bound constraint function (17), the saturation function Sat$[\cdot]$ is

$$\mathrm{Sat}[u,\mathbf{x};t]=\begin{cases} u(t), & \mathbf{c}\le 0 \\ c_{max}\dot{r}(t), & \mathbf{c}>0 \text{ and } |\dot{r}(t)|\le \frac{u_{max}}{c_{max}} \\ u_{max}\mathrm{sgn}[\dot{r}(t)], & \mathbf{c}>0 \text{ and } |\dot{r}(t)|> \frac{u_{max}}{c_{max}} \\ 0, & \mathbf{c}>0 \text{ and } u(t)\dot{r}(t)<0 \end{cases} \tag{20}$$

B. Transient disturbance model

Because transient response to pulse-like excitation is of primary concern in this application, the base acceleration is obtained from the expression for base velocity

$$v(t)=V_p\exp\left[\frac{-\pi^2}{4}\left(\frac{t-2N_cT_p}{N_cT_p}\right)^2\right]\cos\left(2\pi\frac{t-2N_cT_p}{T_p}\right) \tag{21}$$

where the pulse has a period of T_p, a velocity amplitude of V_p, and contains N_c cycles. The base acceleration w is found by differentiating (21) with respect to time using central differences. In all cases, the final time is selected as $t_f = 4N_cT_p$ to ensure all transient simulations were carried out for a sufficiently long duration so as to capture the peak response. V_p and N_c are taken to be 1.0 m/s and 2, respectively.

C. Comparison to passive linear viscous damping

Semi-active damping systems are advantageous only in so far as they can out-perform passive damping systems. In order to assess these advantages, pulse response transmissibilities for the optimal semi-active systems are assessed in comparison to a set of passively damped systems in which the damping forces follow a linear relationship with velocity. The dynamics of the passive system are described by

$$\ddot{r}+2\zeta\dot{r}\sqrt{g\alpha}+g\alpha r=-w \tag{22}$$

where ζ is the dimensionless damping ratio taken to range from 0.15 to 0.7.

IV. RESULTS

The primary objective of this study is to investigate the potential for parameterization of the optimal semi-active control actions in the form of a feedback control law. First, the convergence to similar optimal trajectories from various initial conditions is investigated. Next, the saturation limits of the controls are shown to depend on the choice of c_{max} and u_{max} producing qualitatively different optima, and a parameterized feedback control law is proposed. Finally, a parameter study is undertaken, and peak responses and device forces for a range of pulse periods are presented in Figure 4 along with comparisons to passive linear viscous damping. These pulse response spectra show the dynamic amplification in terms of relative displacement, $\max|r(t)|$, total acceleration, $\max|\ddot{r}(t)+w(t)|$, and device force, $\max|f(t)|$.

A. Convergence from different initial conditions

To assess the ablility of the proposed method to converge to optima, control trajectories originating from various initial guesses were compared. The nonlinear feedback control law initialization method converges to nearly identical optimal trajectories from very different initial guesses. Also, plotting the integral cost function over the iterations showed convergence of the algorithm. The proposed methodology exhibited monotonic convergence to the optimal trajectory independent of initial (feasible) guesses.

The algorithm exhibits sensitivity to the choice of γ similar to an update gain in a gradient descent method. If γ is chosen to be too large the update of the controls can produce infeasible state trajectories. However, if γ is too small, rate of convergence decreases and the method is computationally expensive. Therefore, γ was dynamically determined in order to optimize the iterative process by adaptively reducing γ at a given iteration if the cost increased with respect to the previous iteration.

B. Constrained optimal control

For short period pulses ($T_p < T_n$), a semi-active control law, termed *pseudo-negative stiffness*, is nearly optimal in the absence of control acceleration saturation limit, i.e., $\max|u| < u_{max}$. A pseudo-negative stiffness relationship is when the normalized damper force f has the same sign as velocity $\dot{r}$ and magnitude of the stiffness force $|mg\alpha r|$. Based on the results shown in Figure 3(a), a parameterized control rule for semi-active damping may be proposed as follows:

$$u(r,\dot{r})=krH(-r\dot{r}) \tag{23}$$

where k is feedback gain to be optimized and $H(\cdot)$ is the Heaviside step function. However, when the max control acceleration becomes saturated, the peak control accelerations are clipped, Figure 3(a). Therefore, in order to fully realize a pseudo-negative stiffness feedback control rule, the damper must be designed to achieve force levels that are high enough to avoid saturation.

For excitations near resonance ($T_n/\sqrt{2} < T_p < 1.2T_n$) a damper must be designed with a large admissible control force to avoid saturation due to the large isolator responses. It is in this range of pulse periods that the control law transitions from pseudo-negative stiffness to passive viscous damping as illustrated in Figures 3(b) and 3(c). For long period pulses ($T_p > T_n$), linear damping similar to passive viscous damping, is characterized by an elliptical force displacement relationship seen in Figures 3(c) and 3(d). The effects of clipping are still present for low u_{max}.

C. Parameter Study

In order to compare peak responses and peak device forces the following set of dimensionless variables are formed in

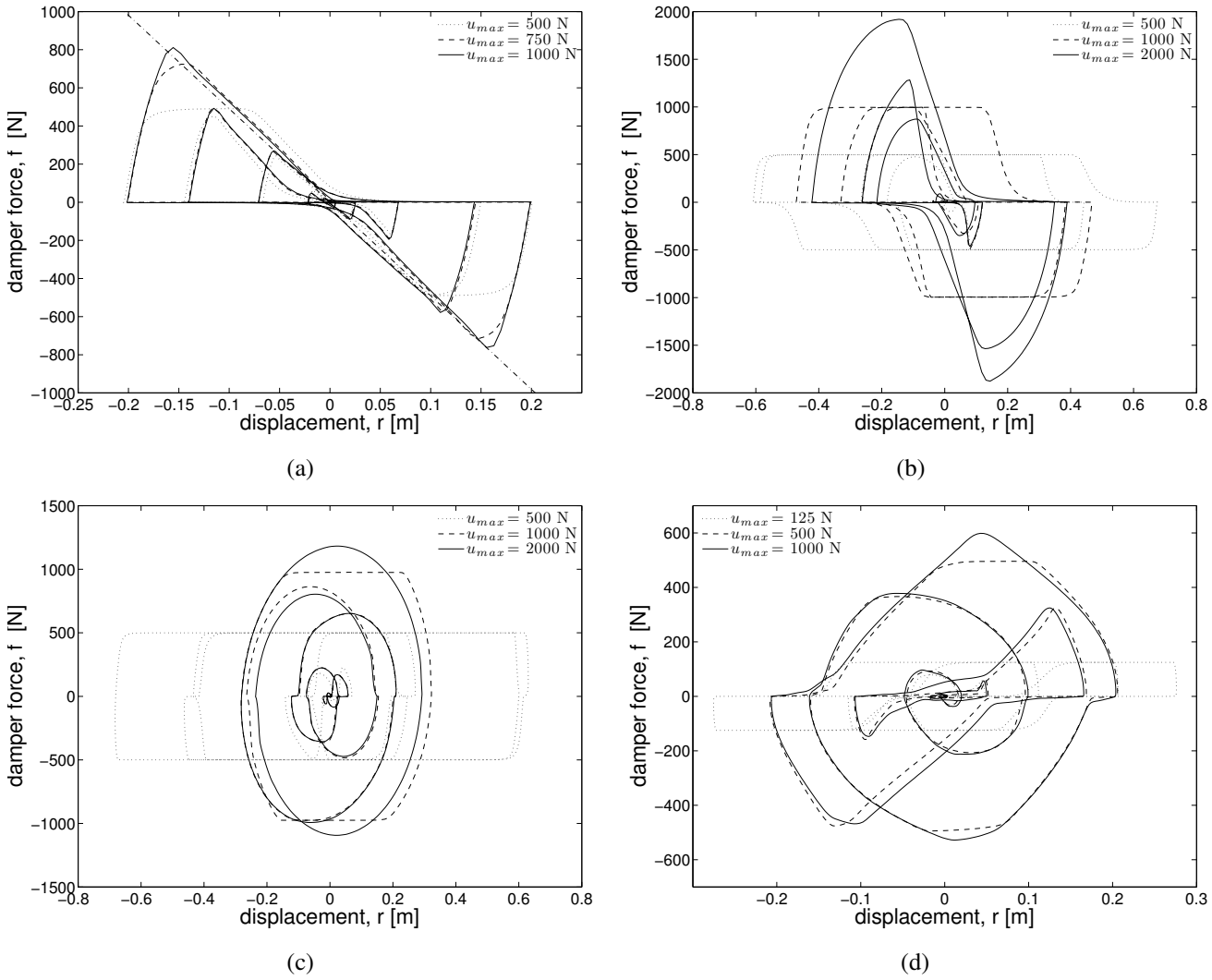

Fig. 3. Saturation of controls by varying u_{max} with $c_{max} = 1500$ N/m/s and (a) $T_p = 1$ s, (b) $T_p = 1.6$ s, (a) $T_p = 2.4$ s, and (a) $T_p = 3.6$ s.

order to perform a parameter study.

$$\Pi_1 = \max|\ddot{r} + w| \,/\, \max|w| \tag{24}$$

$$\Pi_2 = \max|r| \,/\, \max|w_r| \tag{25}$$

$$\Pi_3 = \max|f| \,/ (m \max|w|) \tag{26}$$

$$\Pi_4 = T_p/T_n \tag{27}$$

where w_r is the base displacement.

Figure 4 illustrates the pulse response spectra of the total acceleration Π_1, the relative displacement Π_2, and the device force Π_3 for optimal semi-active damping and linear viscous passive damping. The device force for linear viscous passive damping is $f = 2\zeta\dot{r}\sqrt{g\alpha}$. Figures 4(b)-(c) and 4(e)-(f) show that increasing levels of passive damping, ζ, monotonically reduces peak relative displacements and monotonically increases the peak required damper forces for all periods. However, it is seen that peak response accelerations increase with increasing passive damping for short periods ($\Pi_4 < 1/\sqrt{2}$).

Two values of c_{max} were investigated—$c_{max} = 470$ and 2193 N/m/s, i.e., damping ratios of 15% and 70%, respectively. For short excitation periods, both cases of optimal semi-active damping exhibit lower peak accelerations than any of the passive damping cases. The relative displacement for short periods is comparable to the lightly passively damped cases ($\zeta = 0.3$). Reduced relative displacements are not seen because the quadratic objective function aims to minimize controls and total accelerations, not displacements.

At pulse periods near resonance ($1/\sqrt{2} < \Pi_4 < 1.5$), the optimal semi-active control subject to more restrictive constraints ($c_{max} = 470$ N/m/s) performs worse than the less constrained case ($c_{max} = 2193$ N/m/s) as would be expected. As illustrated in Figures 4(c) and 4(f), the maximum achievable device force is not saturated as frequently for lower c_{max} because the isolator velocities do not exceed u_{max}/c_{max}. Further, the displacement capacity is comparable to the more lightly damped ($\zeta = 0.15$) passive system for $c_{max} = 470$ N/m/s independent of u_{max}. Whereas, the displacement capacity for $c_{max} = 2193$ N/m/s

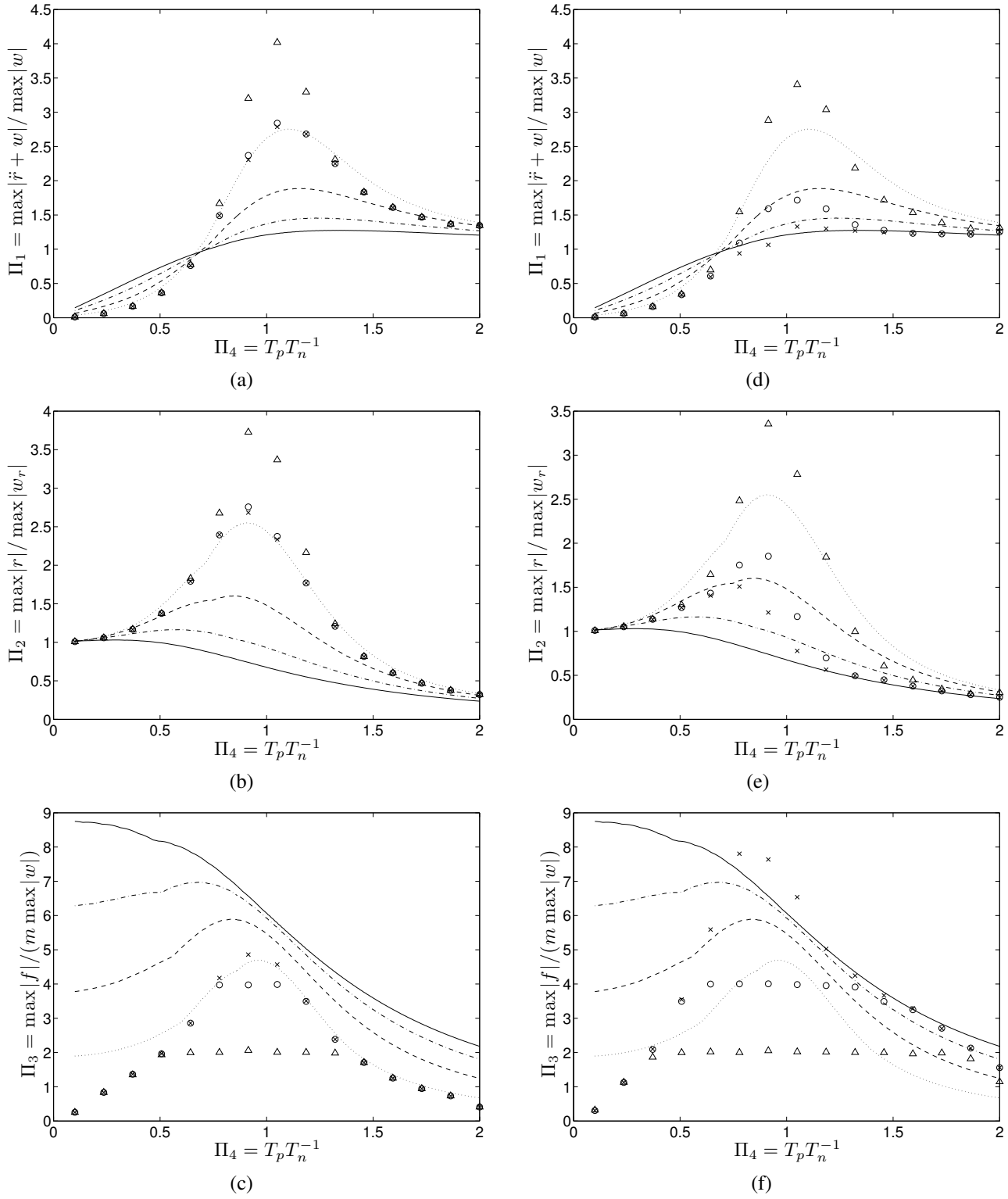

Fig. 4. Pulse response spectra of peak total acceleration (a) and (d), peak relative displacement (b) and (e), and peak device forces (c) and (f) for two sector bounds: (a)-(c) $c_{max} = 470$ N/m/s and (d)-(f) $c_{max} = 2193$ N/m/s. Legend: $\cdots$ $\zeta = 0.15$, $- - -$ $\zeta = 0.3$, $- \cdot -$ $\zeta = 0.5$, —- $\zeta = 0.7$, $\triangle$ $u_{max} = 500$N, $\circ$ $u_{max} = 1000$N, and $\times$ $u_{max} = 2000$N.

with high force capacity ($u_{max} = 1000$ and 2000 N) is similar to the lightly damped passive system with $\zeta = 0.3$ over $1/\sqrt{2} < \Pi_4 < 1$ and the heavily damped system ($\zeta = 0.7$) over $1 < \Pi_4 < 1.5$. Moreover, in terms of total acceleration, the weakly constrained optimized semi-active systems ($c_{max} = 2193$ N/m/s, $u_{max} = 1000$ and 2000 N) show little resonant behavior.

V. CONCLUSIONS AND FUTURE WORK

A. Conclusions

For linear systems subject to nonlinear constraints on states and controls, we have developed a procedure to determine optimal control trajectories based on the minimization of a quadratic performance index. Note that the controls converge to trajectories that are sometimes constrained, but that these controls were determined from costates that did not recognize the presence of constraints, since λ is set to zero for all iterations. Additional performance gains may therefore be achieved from a method that enforces constraints with Lagrange multipliers. Such a method is much more difficult to implement; our implementation did not always converge due to inconsistencies between states and saturated controls; and we expect performance gains of such a method to be slight. To evaluate the performance of the proposed method, the response behavior of a single-degree-of-freedom equipment isolation system is investigated for a pulse-like base-acceleration excitation. Results presented in this paper support the following conclusions:

- The proposed method is effective in determining solutions to the Euler-Lagrange equations describing optimal semi-active control in linear isolation systems. Also, the method exhibits monotonic convergence to an optimal trajectory and is robust to variation in initial guesses.
- At low pulse periods, a pseudo-negative stiffness friction control is optimal in suppressing response accelerations of the isolated component. Whereas, at higher pulse periods, linear viscous damping is optimal. Parameterized feedback control laws are proposed for difference excitation frequencies.
- Pulse response spectra of the optimally controlled isolation system exhibit reduced dynamic amplification in terms of acceleration response. By not saturating the controllable damper, resonant effects are suppressed as well.

B. Future Work

Future work will address higher dimensional systems for isolation of objects oscillating in the horizontal plane. By linearizing the dynamics of the horizontal translations and rotation of the isolated component, optimal trajectories for the semi-active control of a rolling-pendulum equipment isolation system will be found using the proposed methodology. Optimal control performance computed using dynamic programming will be compared to passive damping methods. Also, parameterized feedback control laws will be optimized via parametric optimization methods.

VI. ACKNOWLEDGMENTS

The authors gratefully acknowledge the contribution of the National Science Foundation and reviewers' comments.

REFERENCES

[1] Stengel, R.F. (1994). *Optimal control and estimation*, Dover, New York.

[2] Bryson, A.E., and Ho, Y.C. (1975). *Applied optimal control: Optimization, estimation, and control*, Hemisphere, Washington, D.C.

[3] Borrelli, F., Boatić, M., Bemporad, A., and Morari, M. (2005). "Dynamic programming for constrained optimal control of discrete-time linear hybrid systems." *Automatica*, **41**, 1709–1721.

[4] Mayne, D.Q., and Schroeder, W.R., (1997). "Robust time-optimal control of constrained linear systems." *Automatica*, **33**, 2103–2118.

[5] Bemporad, A., and Morari, M., (1999). "Control of systems integrating logic, dynamics, and constraints." *Atuomatica*, **35**, 207–427.

[6] Morari, M., and Barić, M., (2006). "Recent developments in the control of constrained hybrid systems." *Computers and Chemical Engineering*, **30**, 1619–1631.

[7] Bojkov, B., and Luus, R. (1996). "Optimal control of nonlinear systems with unspecified final times." *Chemical Engineering Science*, **51**(6), 905–919.

[8] Alhan, C., Gavin, H.P., Aldemir, U. (2006). "Optimal control: Basis for performance comparison of passive and semiactive isolation systems." *Journal of Engineering Mechanics*, **132**(7), 705–713.

[9] Gavin, H.P., and Alhan, C. (2005). "Guidelines for low-transmissibility semi-active vibration isolation." *Smart Materials and Structures*, **14**, 297–306.

[10] Symans, M.D., and Constantinou, M.C. (1999). "Semi-active control systems for seismic protection of structures: a state-of-the-art review." *Engineering Structures*, **21**, 469–487.

[11] Sadek, F., and Mohraz, B. (1998). "Semiactive control algorithms for structures with variable dampers." *Journal of Engineering Mechanics*, **124**(9), 981–990.

[12] Sastry, S. (1999). *Nonlinear Systems: Analysis, Stability, and Control,* Springer-Verlag.

[13] Gavin, H.P., and Zaicenco, A. (2007). "Performance and reliability of semi-active equipment isolation." *Journal of Sound and Vibration*, **306**, 74–90.

[14] Lopez Garcia, D., and Soong, T.T. (2003). "Sliding fragility of block-type non-structural components. Part 1: Unrestrained components." *Earthquake Engineering and Structural Dynamics*, **32**, 111–129.

[15] Lopez Garcia, D., and Soong, T.T. (2003). "Sliding fragility of block-type non-structural components. Part 2: Restrained components." *Earthquake Engineering and Structural Dynamics*, **32**, 131–149.

[16] Hutchinson, T.C., and Chaudhuri, S.R. (2006). "Bench–shelf system dynamic characteristics and their effects on equipment and contents." *Earthquake Engineering and Structural Dynamics*, **35**, 1631–1651.

[17] Lu, L.Y., and Lin, G.L. (2009). "A theoretical study on piezoelectric smart isolation system for seismic protection of equipment in near-fault areas." *Journal of Intelligent Material Systems and Structures*, **20**, 217–232.

[18] Kasalanati, A., Reinhron, A.M., Constantinou, M.C., Sanders, D. (1997). "Experimental study of ball-in-cone isolation system." *Proceedins of the ASCE Structures Conference XV*, 1191–1195.

[19] Kemeny, Z.A., Ball-in-cone seismic isolation bearing, U.S. Patent 5599106, February 4, 1997.

[20] Myslimaj, B., Gamble, S., Chin-Quee, D., Davies, A. (2003). "Base isolation technologies for seismic protection of museum artifacts." *The 2003 IAMFA Annual Conference in San Francisco, Calirfornia.*

[21] Iwan, W.D. (1978). "The earthquake design and analysis of equipment isolation systems." *Earthquake Engineering and Structural Dynamics*, **6**, 523–534.

[22] Xu, Y.L., Liu, H.J., Yang, Z.C. (2003). "Hybrid platform for vibration control of high-tech equipment in buildings subject to ground motion. Part 1: Experiment." *Earthquake Engineering and Structural Dynamics*, **32**(8), 1185–1200.

[23] Xu, Y.L., Li, B. (2006). "Hybrid platform for high-tech equipment protection against earthquake and microvibration." *Earthquake Engineering and Structural Dynamics*, **35**(8), 943–967.

[24] Kelly, J.M. (1999). "The role of damping in seismic isolation." *Earthquake Engineering and Structural Dynamics*, **28**, 3–20.

[25] Nagarajaiah, S., and Narasimhan, S. (2006). "Smart base isolated benchmark building part II: Phase I sample controllers for linear isolation system." *Journal of Structural Control and Health Monitoring*, **13**(2–3), 589–604.